Available online at www.sciencedirect.com

ScienceDirect

Procedia Structural Integrity 24 (2019) 978–987

Structural Integrity Procedia

www.elsevier.com/locate/procedia

AIAS 2019 International Conference on Stress Analysis

Fatigue damage on CFRP plates under bending by thermographic and UT analysis, aided with FEM-DIC prediction

Vito Dattoma[a], Francesco Panella[a]*, Alessandra Pirinu[a], Alessandro Castriota[a]

[a]*Department of Engineering for Innovation, University of Salento, Lecce 73100, Italy*

Abstract

In this article, a combination of numerical and experimental methodology for delamination evolution analysis on unidirectional CFRP elements under fatigue is suggested. Fiber-reinforced composite structures exhibit continuous damage accumulation with degradation of effective mechanical properties during cyclic HCF loads. Since advanced composites applications are allowed after extensive experimental certification tests, proposed work is based on experimental procedures to better detect and predict damage initiation and growth, monitoring static displacements and strains under 4-points bending by digital image correlation and measuring compliance variation under fatigue. In addition, non-destructive investigation of composite plates is conducted during cycling tests by using infrared thermography and ultrasonic measurements to detect damage location and validate FEM predictions. Experimental results are analyzed and compared, employing also digital image correlation technique; in addition, thermographic and ultrasonic monitoring inspection with Matlab elaborated measurements are implemented to check results for fatigue damage analysis of same specimens.

Keywords: CFRP; bending test; Cohesive Zone Modeling; delamination; FEM; Damage Evolution.

* Corresponding author. Tel.: +39 (0)832 297786; fax: +39 (0)832 297768.
E-mail address: francesco.panella@unisalento.it.

10.1016/j.prostr.2020.02.085

1. Introduction

Recent research of lightweight and highly reliable transportation needs the excellent mechanical properties of fiber-reinforced composite (FRC) - with carbon and glass fibers as reinforcing materials - in terms of specific strength and stiffness. Many researchers investigated in-plane strength of composites but predicting out-of-plane or through-thickness strength has become important due to increase of applications to thick-walled or curved structures under torsion or bending. In aerospace field, bending fatigue may occur throughout service life and generate progressive damage (either for matrix and inter-layer zone), leading to eventually delaminations, reduction of load carrying capability or catastrophic failure. Recently numerous studies investigated delamination propagation, resulting mainly from opening mode (mode I) fatigue deformation. In fact, delamination or plies separation represents one of the most common failure modes in laminates (Raju, 2008), related to previous micro-damage mechanisms between layers or in off-axis plies. Therefore, delamination resistance and mechanical behavior study under both quasi-static and cyclic fatigue loads is necessary for design purposes, damage tolerance approaches and service life predictions. Several authors studied out-of-plane static and fatigue strength of composite materials using flatwise tension specimens based on ASTM Designation. Fujimoto et al. (2016) examined the out-of-plane static tensile strength of CFRP composites after low cycle fatigue tests, testing L-shaped specimens by four-point-bending method. However, most of the studies examined unidirectional (UD) composite materials, thus in this research, the authors have monitored in real-time thick aeronautical CFRP laminates of simple geometry in order to investigate the damage cumulating up to delamination under fatigue loads. Fatigue tests are conducted by four-point-bending method and a combination of numerical and experimental methods for the damage evolution analysis on unidirectional CFRP elements under fatigue is suggested. A numerical model has employed to describe experimental mechanical behavior of static bending test and damage evolution of specimens, in accordance with ASTM D7264M – 07.

Thermographic and ultrasonic inspections are employed to detect temperature rise of composite specimens in critical zones during cyclic tests; thermal images and time domain signal of specimens have been recorded and then transferred to image processing program which has been developed using MATLAB. Because of their methodological versatility and wide field-application in recent years, DIC approach is also used to correlate deformations to FEM predictions and experimental data, since resulted in a wide and quick diffusion in academic areas. Therefore, authors utilize open source platform to obtain localized static displacements on specimen transversal surface under study; data elaboration and first post-processing obtained results are finally discussed.

Nomenclature

F_{Amp_norm}	normalized amplitude fatigue load	F_{max_norm}	normalized maximum fatigue load
K_{norm}	normalized stiffness	N_{norm}	normalized fatigue number of cycles

2. Materials and experimental methods

Fatigue tests are conducted by four-point-bending method using unidirectional CFRP laminated composite bars of rectangular cross section [Dim. 130 × 39 × 6.78 mm], supported as a beam, and fatigue strength is examined. Mechanical properties of matrix and reinforcement materials are presented in the Table 1. The CFRP composite laminate for specimens is composed by 32 plies symmetrically arranged in angle-ply configuration; lamination sequence is $[+45, -45,0,90]_{4s}$ and realized through Liquid Resin Infusion process for aeronautical manufacturing studies. Table 1 also shows resulted laminate employed for FEM simulations. Mechanical bending tests have been carried out on a servo-hydraulic testing machine INSTRON 8850 having a load capacity of 250 kN in Experimental Mechanical Laboratory at University of Salento (Lecce, Italy). Specimens are tested following experimental experience and indication of ASTM Standard D7264M – 07 for Flexural Properties of composites. Distance L (Fig. 1a) is equal to 100 mm due to specimen dimensions. Loading noses and supports shall have cylindrical contact surfaces of radius 3.00 mm [0.125 in.] as shown in Fig. 2a, with ground surfaces free of indentation and all sharp edges relieved, arranged in setup shown in Fig. 1b. Preliminary static tests (specimens P0) provide maximum bending breaking load (F_{static}) and relative displacement (u_{static}), used as reference value for fatigue tests, to evaluate initial stiffness and compare residual fatigue stresses and static FEM model's results, for validation.

Ten fatigue tests are performed with load frequency 4 Hz and stress ratio R = 0,05. In Table 2, experimental parameters (normalized amplitude and normalized maximum load load) are chosen constant during test and fatigue failure mode of

specimens are reported. Experimental overview of fatigue bending tests shows general data variation in damage modes due to test variability, but after tests, even that different fatigue failure zones of specimens are evaluated, good coherence of resulting life is observed. In Figure 1b, diagram illustrates resulting trend of maximum test load as function of fatigue cycles' number, where linear behavior is approximately identified in double logarithmic plot.

Table 1. Mechanical/ physical properties of CFRP material constituents.

Property	Fiber	Matrix	Laminae
E_{11} (GPa)	290	3.4	128.638
E_{22} (GPa)	14	3.4	7.336
E_{33} (GPa)	/	/	7.336
G_{12} (GPa)	25	1.25	4.045
G_{23} (GPa)	7	1.25	2.912
T_g (°C)	/	179	/
ν_{12}	0.236	0.43	0.34
ν_{23}	0.011	0.43	0.545
ρ (g/cm^3)	1.785	1.24	/

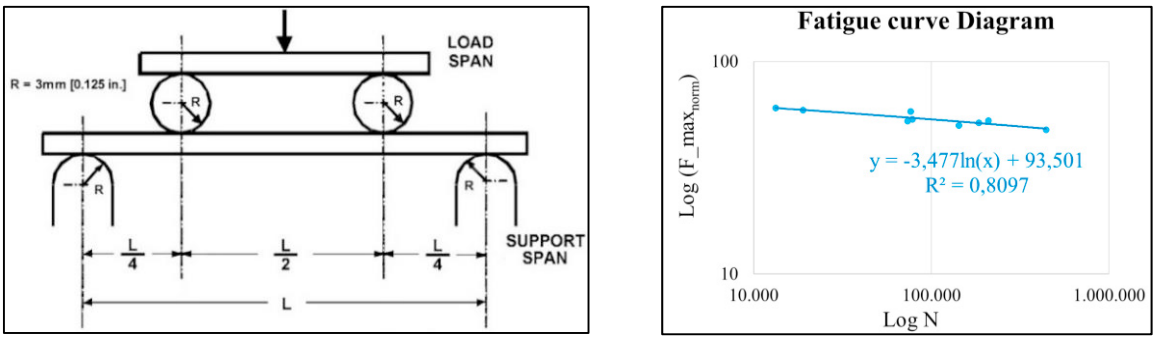

(a) (b)

Fig. 1. (a) Schematic view of four-point bending test ASTM D7264M – 07; (b) fatigue curve diagram.

Table 2. Scheduled experimental results for each fatigue bending tests.

ID	F_{max_norm} [%]	F_{Amp_norm} [%]	N. cycles (N_f)	Damage zone and type
P1	58.30	27.70	71798	Crack at upper left support and delamination in 6° and 16° layers;
P2	53.39	25.34	78316	Delamination in 5° and 16° layers
P3	52.76	24.07	204000	Delamination in 6° and 24° layers
P4	49.96	22.87	142677	Crack on 1° ply; delamination in 2°, 16° and 30° layers
P5	58.96	28.68	18930	Delamination in 10° layer
P6	54.98	26.29	25800	Delamination in 10° layer
P7	47.81	22.07	442561	Undamage
P8	51.39	23.74	185343	Delamination in 6° and 8° layer
P9	52.59	23.90	73696	Delamination in 6° and 10° layers
P10	60.56	29.48	13289	Delamination in 10° layer

3. Damage monitoring methods and numerical model

3.1. Thermographic control

Thermographic controls are performed using a cooled IR camera FLIR X6540sc (Flir System, Inc. Winstonville, OR, USA) with 640×512 pixels. Thermal sequence is acquired with a sample rate of 117 Hz, with an observation time of 10 seconds. It is important to highlight as 117 Hz represents the maximum value of the sample rate selectable from IR camera to acquire frames of whole specimen. An optimum set-up arrangement is proposed as in Fig. 2b, where

specimen is closer to infrared camera and an insulating plastic-foam cover placed behind sample in better position in terms of angles to avoid some reflections and thermal disturbance caused by oil transmission pipes and to achieve best results. For thermographic analysis, a first step consists in reducing thermal environment influence by subtracting an initial image at environmental conditions, taken before starting test, from subsequent images. Therefore, all acquired sequences of images are post-processed with proper Matlab routines. Sequences of ΔT images are created according to equation proposed by Carlomagno et al. (2017)

$$\Delta T(i,j,t) = T(i,j,t) - T(i,j,0) \tag{1}$$

where i, j and t are specific row/column and frame number respectively in the sequence and t=0 the first frame.

As next step, six measurement positions are chosen as regions of interest (ROI) over front surface of over each specimen, three in the upper stretched zone and other three in the bottom compressed zone. As example, Figure 2a shows measurement areas and each rectangle covers 60 × 20 pixels. In each ROI, the average temperature sequence is evaluated frame by frame in order to obtain the temperature evolution over time. Following the assessment that temperature signal plays a determining role in the study of fatigue behavior of CFRP material, in the frequency domain the simplest analytical model is represented by equation:

$$T(i,j,t) = T_0 + b * t + T_1 * sin(\omega * t + \pi + \varphi) + T_2 * cos(2 * \omega * t + \psi) \tag{2}$$

Where 'T_0 + b*t' represent long lasting temperature evolution for linear fatigue life variations, ω is the angular frequency of mechanical imposed load, T_1 and φ are respectively related thermo-elastic signal and T_2 represent the amplitude of second Fourier harmonic component, characteristic of harmonic character for each acquisition, claimed to be proportional to intrinsic energy dissipation; ψ is the phase signal of temperature component. In addition, it possible also to refer to the thermal uncalibrated signal, since the purpose is to assess the variation of the indexes, that are significant when damage conditions occur (Galietti et al., 2016).

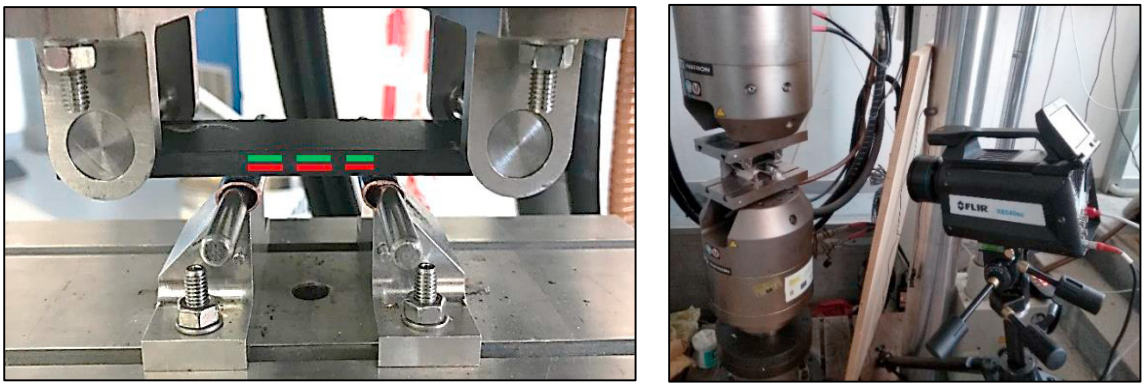

(a) (b)

Fig. 2. (a) Experimental setup with fixed supports and rolling loading supports; (b) thermographic configuration for thermographic controls.

3.2. Digital Image Correlation method

In order to study the force-strain behavior of CFRP samples under bending, experimental static tests are performed in combination with macroscopic digital image correlation analysis within a region of interest (ROI) for a material sample undergoing deformation, employing image processing techniques (J. Blaber et al., 2015). During the displacement-controlled test (displacement rate 2 mm/min), series of images (with a resolution of 4000 × 6000 pixels) are taken at the center of specimen using a Nikon High-resolution camera with macro camera lens. Basically, images are taken throughout test and used as inputs to DIC code available in the market. Due to limitations of inherent costs involved in the restrictions imposed on users, as they cannot modify the source code as per their requirements, an open source software can be modified for user requirements. Ncorr is an open source 2D digital image correlation implemented in Matlab Software (J. Blaber et al., 2015), whose capabilities and reliability has been verified in other works. The free digital software also used for DIC

evaluation is GOM Correlate, developed by "GOM Precise Industrial 3D Metrology" for automated 3D measuring innovative technology. Qualitative comparison between the two DIC software is briefly presented.

3.3. Ultrasonic inspection

Experimental equipment for conventional Ultrasonic Techniques consist of digital oscilloscope (Agilent Technologies DSOX2012A), a Control Unit GE USIP 40 and two axial probes (Olympus A103S-1 MHz frequency and DS 12 HB 1-6 frequency probe as receiver), employed for damage detection on specimen with direct contact UT transmission, interposing a direct coupling gel on CFRP surface. A PLA tool (the green one support in Fig. 3a) allow to ensure the correct and stable parallel arrangement of transducers, easy manipulation and probes orientation, with perfectly aligned axes, guaranteeing identical acoustic energy transmission during fatigue life on specimen.

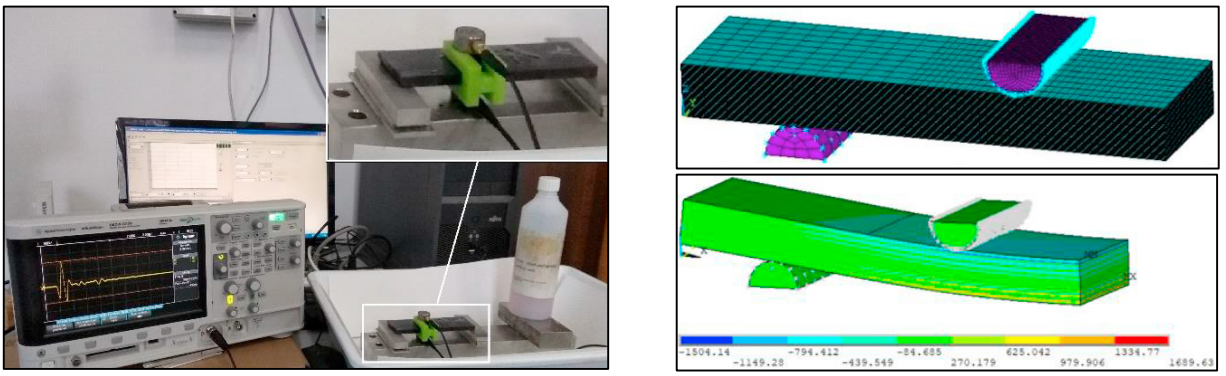

(a) (b)

Fig. 3. (a) Experimental Layout for ultrasonic control set-up; (b) FEM mesh of laminate and σ_x fiber stress distribution.

Latest advances in ultrasonic analysis are based on digital signal processing, for detection of harmonics of higher grade than principal wavelength signal for damage or delamination studies in composites. Non-Linear ultrasonic technique presents the advantage of exceptional sensitivity for initial damage inspection based on micro-changes in material properties and/or micro cracks or localised degradation. This monitoring methods is suitable for initial stage damage mechanisms, i.e. fatigue nucleation with perceptible levels (Ciampa et al., 2015). Authors decided to investigate CFRP specimens at regular intervals during fatigue tests, to record and analyze amplitude [%] signal and time domain behavior of propagating ultrasounds through thickness. This data is then analyzed over the fatigue life to verify possibility of initial damage detection in case of alternate bending of CFRP laminates. Sampling frequency is 2 GSa/s and time domain data in are subsequently elaborated into frequency domain employing a Matlab algorithm based on Fast Fourier Transform (FFT), comparing results with reference signal of unloading specimen.

3.4. Numerical FEM model

When CFRP specimen will be subjected to fatigue bending load and need stay in local contact with the outer area of metallic supports, such as in this work, FEM Calculation offers detailed stress and deformation changes in the critical regions of interest. A FEM model is realized with numerical software in order to predict the progressive damage of preliminary static bending test. A 3D model is built, the interface between laminae is modelled using a Cohesive Zone Model, implementing an exponential behavior law for FEM simulation of initial interface delamination. Coupled cohesive zone law is required, in this case adopting the exponential form originally proposed by Xu and Needleman (1993), generally proved to be the most efficient:

$$\phi(\delta) = e * \sigma_{max} * \bar{\delta}_n * \left[1 - \left(1 + {\delta_n}/{\bar{\delta}_n}\right) * e^{-{\delta_n}/{\bar{\delta}_n}} * e^{\left(-{\delta_t}/{\bar{\delta}_t}\right)^2}\right] \tag{3}$$

Where $\phi(\delta)$ is surface potential; e is a constant; σ_{max} the maximum normal traction at the interface; $\bar{\delta}_n$ the normal separation across the interface where the maximum normal traction is attained with $\delta_t = 0$; $\bar{\delta}_t$ the shear separation where the maximum shear traction is attained at $\delta_t = \sqrt{2} * \bar{\delta}_t/2$. In this work, the maximum normal traction σ_{max} of

the material is estimated to be 30 [MPa] and the normal (δ_n) and tangential (δ_t) opening shifts are evaluated in 16 $\times 10^{-3}$ mm and 12 $\times 10^{-3}$ mm respectively, after previous numerical studies on similar material.

In the FEM software the cohesive zone is modelled by interface elements between plies and, to reduce the calculation time required for each individual simulation, only a quarter of specimen (Dim. 65 × 18 × 6.78 mm) is modeled using double symmetry of geometry, loads and constrains. As in Fig. 3b, the mesh is divided into two main regions: a more detailed mesh corresponding to nearest supports and remaining region with a coarser mesh. The model thus generated aims to provide an accurate representation of 3D stress field developed around supports, due to pure bending effects (as in Fig. 3b) and related through-thickness contact pressures in support contact regions. This model allows the accurate addressing of all 3D damage types, including compressive/tension matrix collapse, shear slips in x and y directions, leading to delamination; maximum directional strain and Hashin-type failure criteria (Hashin, 1980) are used to predict matrix and fiber damage. Initial delamination effect is included in a successive calculation and its effects are considered only in the initial cracking phase, before convergence is lost.

4. Discussion of results

4.1. Experimental test results

Preliminary static test is accurately recorded by camera photos and images processed with two DIC software. In Fig. 4, similar displacement field contours are displayed in normal and longitudinal direction; thought contour displacements and field strains coincide in both software, some numerical value differences are observed in Ncorr results around -4% from GOM results for the same 4 points, two in the central zone and other one in supports proximity. Comparing experimental results with FEM model predictions, CFRP may be considered damaged realistically well before maximum F_{static} is reached, adopting both Hashin and maximum strain criterion.

For FEM analysis, in static case with maximum strain criterion, fibres breaking occurs already with load lower of -12% than F_{static}, while Hashin criterion predicts load smaller of -14.7%. These numerical values are not considered for fatigue composite failure evaluation, but as reference values when first damage is likely to occur with deviation behaviour from linear load curve, generated by σ_y (Fig. 5a), fibre breaking, shear breaking σ_{xy}, and σ_{zy}, and finally initial delamination. Stresses state shows a localized failure in 3rd and symmetrically in 30th layers with maximum strain criterion, while in Hashin FEM model the initial failure occurs in 30th to 32th lower layers (Fig. 5a). However, both FEM models show severely damaged layers in traction layers, verified with experimentally observed damage on broken samples and after static DIC analysis; in Fig. 5b, ε_y strain values increase before initial delamination occurs.

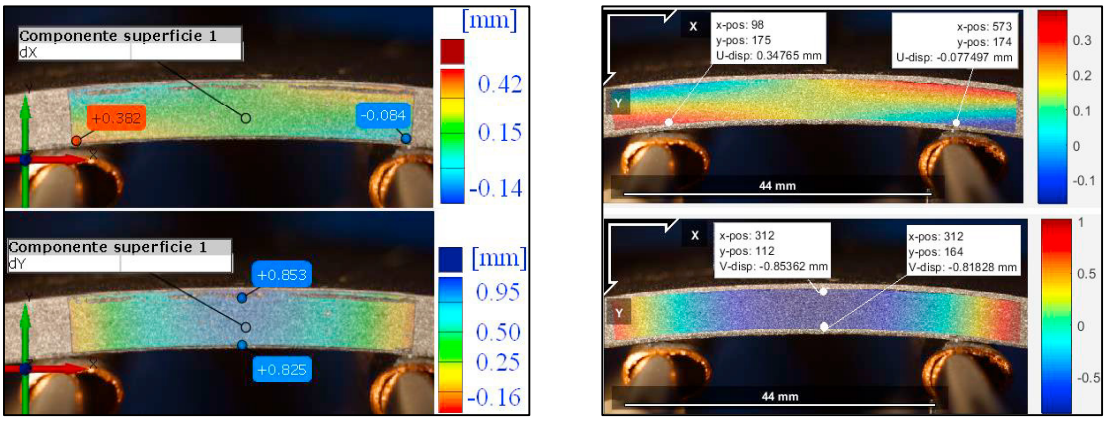

(a) (b)

Fig. 4. (a) X and Y displacement contours for specimen P0 under bending static test obtained with GOM and (b) Ncorr Matlab software.

From diagram shown in Fig. 6a, static test curves in the initial linear trend show small differences between numerical and experimental values; from histogram in Fig. 6b, initial loading phase shows small stiffness difference between Hashin, maximum strain and cohesive zone model, as compared to experimental value, which underestimate results; however, the maximum strain model seem to offer an optimal behavior in general. In the main static load curve section, Hashin criterion seems to present better behavior because the difference between the initial stiffness

values is almost irrelevant; whilst in the last loading section the opposite occurs, i.e. there is a better correspondence with the maximum deformation criterion, since the two stiffness values differ by 0.23%, while Hashin criterion gives 7% error. From what concerns fatigue tests, different fatigue failure and progressive damage of specimens are encountered for each sample surface and classic fatigue damage is evaluated by means of displacements variation during life, i.e. compliance analysis. Figure 7a shows stiffness variation for all sample under fatigue, throughout fatigue life, where the stiffness has been normalized respect to initial value and number of cycles to total life.

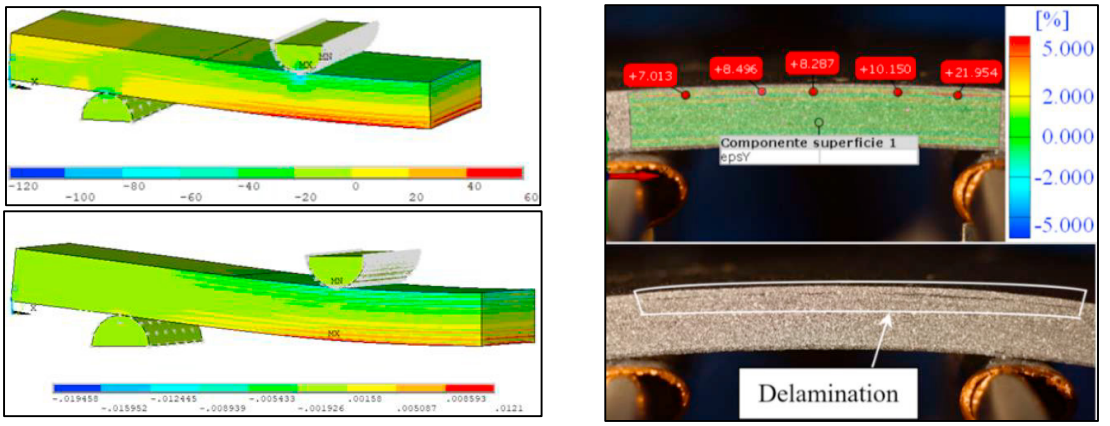

(a) (b)

Fig. 5. (a) Hashin stress σ_y (up) and maximum strain (bottom) matrix plots; (b) GOM ε_y strain contour for specimen P0 and delamination.

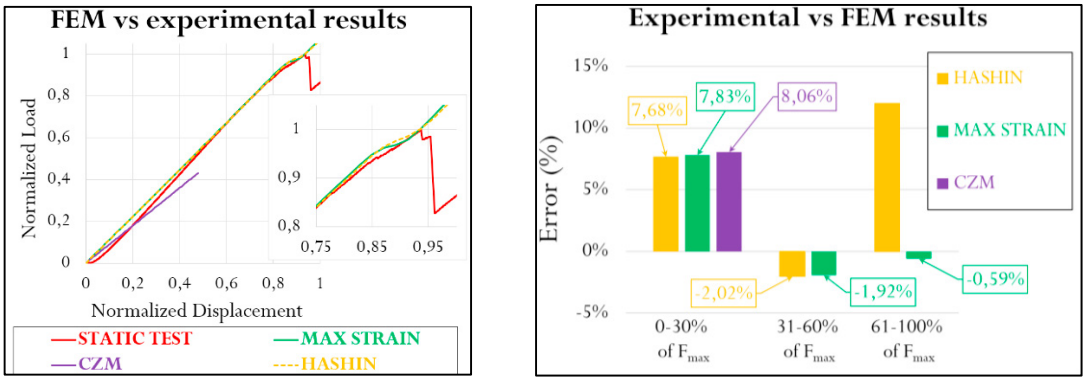

(a) (b)

Fig. 6. (a) Comparison of FEM and experimental static results; (b) FEM stiffness error results between failure criteria.

During tests, data are recorded with a frame rate of 10 Hz and fatigue results show significant stiffness reduction increasing load cycles number; before fatigue damage stiffness decay occurs, all samples shows a rapid decrease in the initial phase, followed by stabilized general trend in central part of test and a further decrease in the final phase, because of progressive damage accumulates before final delamination occurs in specimen's thickness. Generally, 85% of total fatigue life is ensured before delaminations start to occur until sudden specimen failure, with collapse of both tensile and compressive stresses that induce macro defects generation. In some cases, the stiffness trend is interrupted abruptly without undergoing a further stiffness reduction, as seen for P5 and P7, due to low level of applied load. Samples P1, P3, P4 and P7 are subsequently tested statically to assess their residual stiffness and several results are compared with the preliminary static test, as reported in Fig. 7b and 7c; as shown in the diagram, the stiffness of samples P7 and P0 are similar and force displacement shows an identical trend, therefore this sample is considered undamaged and static test is stopped at 55% of F_{static} load for future developments. In addition, static tests on the specimens P1 and P7 are taken by camera for DIC analysis to check strains in the central region with GOM software. As indicated in Fig. 8, the Y vertical displacements of two points chosen on stretched fibers layer (upper layer) and on compressed fibers (bottom layer) show two curves with a similar trend up to 90-95% of the static test of specimens

P0 and P1, until displacement difference Δv occurs for delaminations among plies. Point curves of sample P7 specimen do not show any Δv because macro delamination is absent and therefore specimen thickness is not modified after static test.

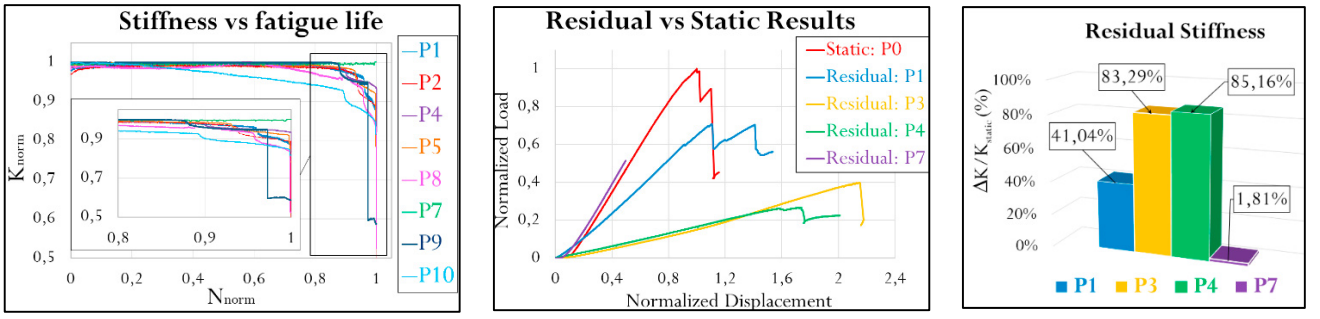

(a) (b) (c)

Fig. 7. (a) K_{norm} vs N_{norm} for some fatigue tests; (b) static vs residual bending results; (c) comparison of residual stiffness.

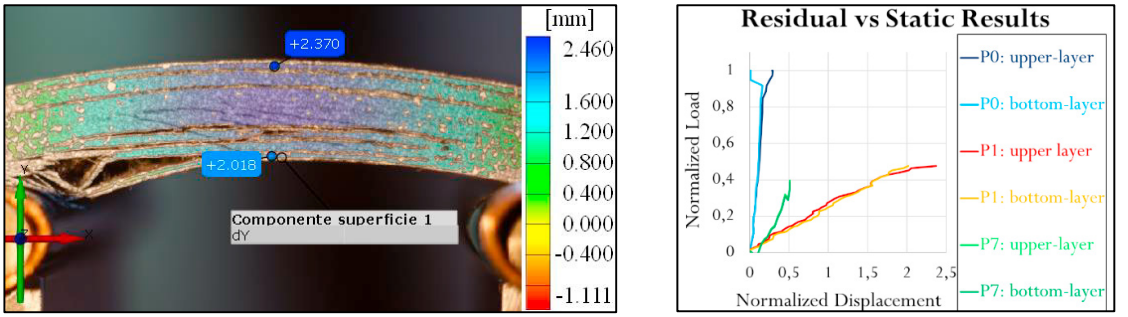

(a) (b)

Fig. 8. (a) V displacement contour obtained for residual static test of specimen P1 using GOM; (b) V displacement results for P0, P1 and P7.

4.2. ND monitoring results – Analysis of the damage

During fatigue tests, authors monitored only samples P5, P8, P9 and P10 with thermographic and UT control acquisitions during life. Different stress field between layers creates different heat generation which increases the temperature from reference undamaged image as function of fatigue life; this thermal event may show damaged zones as visible by thermal imaging, as in Fig. 9a for specimen 10. T_0 parameter estimated as in eq. 2 is compared with reference initial value at 0% of fatigue life and ΔT trend versus time in whole experimental tests is reported in Fig. 9b; in particular, each ΔT plot is obtained as average value over a 1200 pixels' area by timed acquisitions of 10 seconds. Measured ΔT profiles of two selected central areas (one in upper layers and other one in bottom layers) over fatigue life are compared for each specimen, as temperature at different stages of normalized cyclic loading, to highlight in ROIs surrounding the initial delamination process of four specimens subjected to different stress levels, as in Table 2. Similar thermal profiles and higher temperature values are found for P8 and P9, subject to F_{max_norm} equal respectively to 51.39% and 52.59%. For all samples, at the initial cyclic loading, considerable heat generation and thermal increase is observed for all ROI, and subsequently an equilibrium temperature is maintained up to 80% approximately of life, when some thermal gradient irregularities are present in recorded signals and final sudden thermal increase of 4 to 5°C occurs in last phase of failure.

Raw average thermal signals of samples are processed as in eq. 2 and examples T_1 and T_2 variations parameters are shown in Fig. 9c and 10a, extracted from two different zones over central front surface of P9 specimen (as in Fig. 2a). Signal amplitude shows a decreasing behavior during 95% of total fatigue life until a sudden abrupt jump occurs, presumably caused by large delamination as shown in fig. 5b. Comparing these data to other thermo-elastic signals reported in Fig. 10a from other specimens in the tensile upper layers, it is possible to recognize the abrupt jumps only for the P8 and only in the last cycles; similar amplitude and higher value for compression zones are also observed. In previous works (Galietti et al., 2017), T1 and T2 parameters, associated with 1st order thermo-elastic effect and 2nd order damage energy association, are

capable to detect initial damage progression, well before failure. In our case, on the other hand, the instrument noise strongly affects the temperature variations induced by the cyclic bending conditions, which is tried to be determined along specimen section through thickness. Evident delamination occurrence is clearly distinguished only in the last cycles and for some specimens only, whilst clear indications of damage nucleation is for the moment are missing.

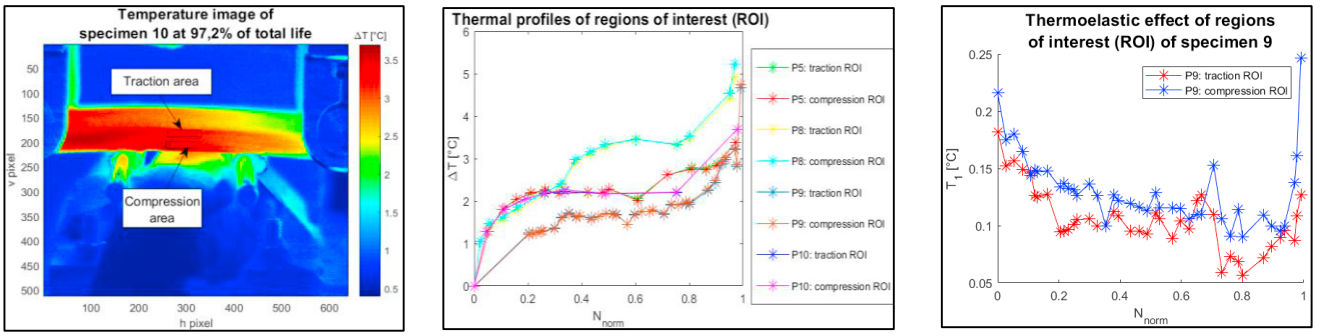

(a) (b) (c)

Fig. 9. (a) Thermal image of fatigue test for specimen P10; (b) thermal profile of selected ROI; (c) thermo-elastic effect of selected ROI in P9.

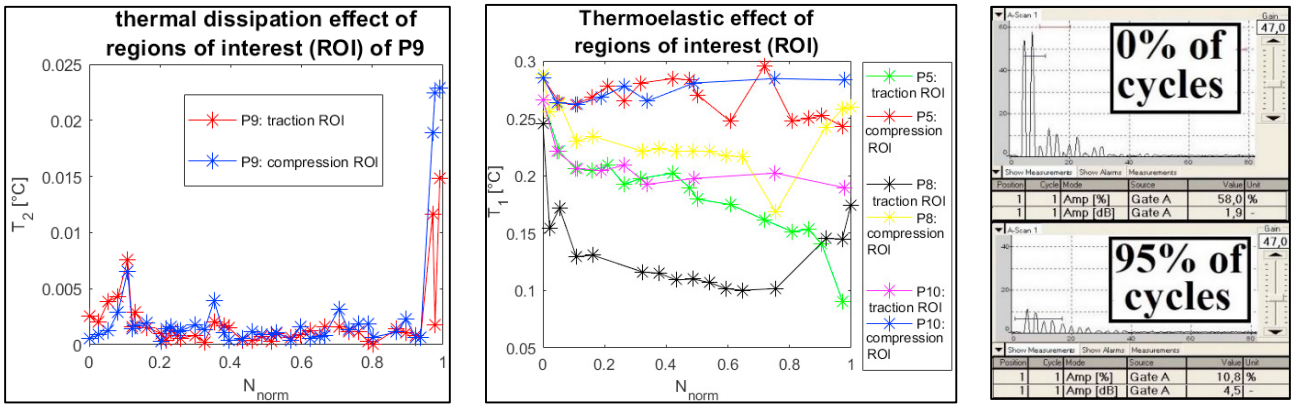

(a) (b) (c)

Fig. 10. (a) Thermal dissipation coefficient of P9; (b) thermo-elastic coefficients for P5, P8 and P9; (c) A-scan of UT inspection of P9.

This is probably due to composite type of specimens under localized bending, or due to ROI dimension and location choice in the small thickness lateral section, which seems for the moment not suitable for fatigue damage prediction before failure. the thermo-elastic effect linked to the specimen oscillation is only measured in tension (cooling down) part, while the rear one is in compression (heating up) show alternate cooling/heating effect. Thermal gradients are elevated and create not uniform temperature distribution in the thickness direction, but a slight percentage of temperature accumulation and differences is observed for the selected central ROIs in all sample.

Ultrasonic technique presents the limitation of difficult development of real time and in-situ UT measurements on specimens due to induced bending deformation state of specimen during fatigue test, geometrical spaces to operate during loading and consequent probe surface damage. UT scans are done on four selected zones on upper surface between closest supports; therefore, amplitude and time domain signal data are recorded on specimen at regular intervals each of 10000 cycles. Resulting data are analyzed as function of fatigue cycles and first results are negligible obtained for shorter fatigue life of P5 and P10 samples, due too large acquisition time interval. Slightly better results are observed in other cases, but only P9 specimen results are interesting and worth to be presented in Fig. 10c and Fig. 11. In both A-scans and signal diagram of Fig. 10c, the reduction of amplitude output signal of P9 structural decay represents an evident indication that there is a discontinuity along the sonic wave path, with respect to the initial reference state, but without having any information regarding its type or causation, despite local delamination is presumed to take place. The same signal behaviour is also observed for sample P8 and not considered really important because is claimed not be associated with initial fatigue damage accumulation. Measuring signal in time domain and studying fundamental frequency amplitude attenuation,

interesting data variation is observed during fatigue life, as reported in Fig. 11a. Acquired signal data are converted into the frequency domain using an algorithm developed in Matlab, based on simple Fast Fourier Transform (FFT) for received signal in dependence of fatigue life. Figures 11b and 11c show the Fourier spectra (FFT) of acquired UT signals and fundamental amplitudes at 1MHz, highlighting an evident frequency attenuation from 0% of reference signal to maximum values of 54, 67, 81 and 95% to be observed. Different evident amplitudes are observed at lower frequency with a shift phenomenon during fatigue life, as in Fig. 11c.

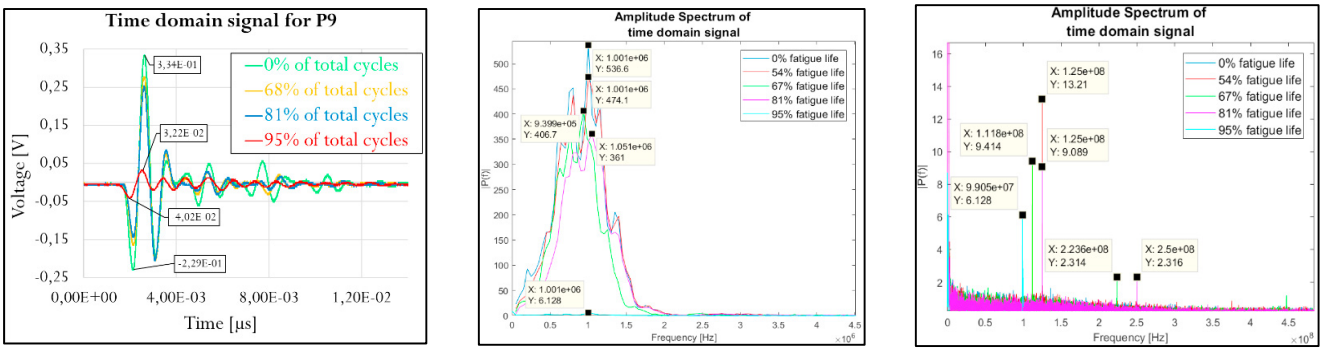

(a) (b) (c)

Fig. 11. (a) Signal in time domain; (b) fundamental amplitudes of frequency spectra; (c) 2nd and 3rd amplitude of P9 during fatigue life.

4. Conclusions

Fatigue experimental results indicated the bending fatigue life of CFRP elements is determined by continuous and early damage evolution and structural specimen state, well before final rupture, as well as the amount of residual static strength and stiffness after fatigue testing on specimen is apparently and with surprise nearly intact. Several damage mechanisms (i.e. matrix cracking under tension in matrix y direction and shear in x-y and z-y planes for initial delamination occurrence) are identified numerically with modelled failure modes and coupled cohesive zone to include small delamination , before fibre rupture and experimental measurements of displacements and strains are verified with enough accuracy; static behaviour is correlated and successively estimation of the progressive fatigue damage evolution is possible when lower load are applied for large number of cycles. An important conclusion is the experimental fatigue life under 4 point bending for aeronautical CFRP settles approximately at 50% load level, with respect to static conditions. In the present work, DIC strain field measurements, thermographic and ultrasonic ND monitoring methods have been employed for damage evaluation throughout experimental tests; initial results are satisfactory, though not complete, since early stages of damage initiation is not easily identified, since through thickness local analysis for different layers appear to be strongly affected by noise and other factors.

References

Blaber, J., B., Adair, Antoniou, A., 2015. Ncorr: Open-Source 2D Digital Image Correlation Matlab Software, *Exp. Mechanics*, 55, 6, 1105-1122.

Ciampa, F., Malfense Fierro, G.P., Ginzburg, D., Meo, M., Onder, E., 2015. Nonlinear ultrasound modelling and validation of fatigue damage, *Journal of Sound and Vibration*, Vol. 343, pp. 121–130.

Carlomagno, G. M., Boccardi, S, Meola, C., Simeoli, G., Russo, P., 2017. Evaluation of polypropylene based composites from thermal effects developing under cyclic bending tests. *Composite Structures*, Vol. 182, 628-635.

Fujimoto, K., Hojo, M., Fujita A., 2016. Low cycle fatigue of CFRP laminated composites due to repeated out-of-plane loading, 21st European Conference on Fracture, ECF21, 20-24 June 2016, Catania, Italy, *Procedia structural Integrity 2*, pp. 182–189.

Galietti, U., Demelio, G. P., Palumbo, D., De Finis, R. 2017. Study of damage evolution in composite materials base on the Thermoelastic Phase Analysis (TPA) method, *Composite part B*, Vol. 117, 49-60.

Galietti, U., Demelio, G. P., Palumbo, D., De Finis, R., 2016. A new rapid thermographic method to assess the fatigue limit in GFRP composites, *Composite part B*, Vol. 103, 60-67.

Hashin, Z., 1980. Failure criteria for Unidirectional fibre composites, *J Appl. Mach 47,* 329-34.

Raju, I. S., 2008. Fracture mechanics concepts, stress fields, strain energy release rates, delamination initiation and growth criteria. In: Delamination Behaviour of Composites. Sridharan, S. (ed.) Woodhead Publishing Ltd., Cambridge, England, 3–27.

Xu, X. P., Needleman, A.,1993.Continuum Modelling of Interracial Decohesion,Dislocations 93,Solid State Phenomena,35, 287-302.